

*promoting access to White Rose research papers*



**Universities of Leeds, Sheffield and York**  
**<http://eprints.whiterose.ac.uk/>**

---

This is the author's post-print version of an article published in the **Quarterly Journal of the Royal Meteorological Society, 138 (666)**

White Rose Research Online URL for this paper:

<http://eprints.whiterose.ac.uk/id/eprint/76543>

---

**Published article:**

Ross, AN (2012) *Boundary-layer flow within and above a forest canopy of variable density*. Quarterly Journal of the Royal Meteorological Society, 138 (666). 1259 - 1272. ISSN 0035-9009

<http://dx.doi.org/10.1002/qj.989>

---



---

# Boundary-layer flow within and above a canopy of variable density

Andrew N. Ross, <sup>a\*</sup>

<sup>a</sup>*Institute for Climate and Atmospheric Science, School of Earth and Environment, University of Leeds*

\*Correspondence to: School of Earth and Environment, University of Leeds, LS2 9JT, UK. Email: A.N.Ross@leeds.ac.uk

---

An analytical model is developed for flow within and above a forest canopy with a slowly varying canopy density. Results are compared with existing analytical models for flow over a surface with slowly varying roughness length, and also with numerical simulations. The results show that the analytical solution is successful in capturing the behaviour of the flow for small and slowly changing variations in canopy density. Previous models which only vary the roughness length and neglect changes in displacement height fail to capture the near surface flow accurately. Including changes in displacement height as well as roughness length changes gives results closer to those obtained with the full canopy model, but even then the flow induced in the canopy leads to significant differences. The analytical model also highlights the sensitivity of the results to the parameterization of the vertical component of the turbulent stress tensor,  $\tau_{zz}$ . For shorter wavelength variations in the canopy density the analytical model breaks down as the more rapid changes in density induce larger flow perturbations which lead to increased flow into and out of the canopy. This kind of idealised analytical study provides important insights into the role of canopy heterogeneities on boundary layer flow. This is important both for understanding near-surface winds and transport, and also for parameterizing the effects of surface heterogeneities in large-scale weather and climate models.

Copyright © 0000 Royal Meteorological Society

*Key Words:* Forest canopy; Inhomogeneous canopy density; Variable surface roughness

## 1. Introduction

For a number of years there has been significant interest in flow through forest canopies. To a large extent this has been driven by a desire to understand transport in and above forest canopies which is important in understanding and measuring fluxes of CO<sub>2</sub>, water vapour, isoprene and other species which are either emitted or absorbed by vegetation. Such canopy dynamics are also important in understanding the effects of surface conditions on low level wind fields and pressure fields, and in determining appropriate parameterizations of these in large-scale weather and climate models. A large amount of this work has focused on homogeneous canopies on flat terrain, however more recently there has been a shift to understanding non-homogeneous canopies and terrain. Lee (2000) gives an overview of some of the earlier work on non-homogeneous canopies. More recently interest has primarily been in the effects of terrain (e.g. Finnigan and Belcher 2004; Ross and Vosper 2005) and of sharp forest edges (e.g. Irvine *et al.* 1997; Morse *et al.* 2002; Yang *et al.* 2006; Dupont and Brunet 2008, 2009; Dupont *et al.* 2008; Romniger and Nepf 2011). In particular Belcher *et al.* (2003) produced an analytical model for flow across a canopy edge using similar methods to those discussed here. In an appendix Coceal and Belcher (2004) considered the related problem of the adjustment of a perturbed canopy flow to its equilibrium values. Rather less attention has been paid to studying the less dramatic, but potentially still important, effects of slowly varying changes in canopy properties, and this will be the focus of the present paper.

Previous studies of slowly varying surface properties tend to use a roughness length parameterization of the vegetative canopy rather than an explicit canopy model. Belcher *et al.* (1990) developed an analytical model for such roughness length changes. Using a Fourier decomposition they studied both sinusoidally varying and step changes in roughness. Numerical studies of slowly varying roughness length include the large-eddy simulations of Hobson *et al.*

(1999). Notably both these studies consider only a change in the roughness length and neglect the effect of any displacement height changes, although (as Hobson *et al.* 1999, point out) the latter are likely to be important in the real world.

Using ideas from the analytical models of Belcher *et al.* (1990) and Finnigan and Belcher (2004) (henceforth BXH and FB respectively) this paper will develop an analytical solution for flow within and above a canopy of variable density. The analytical solution will be compared with existing solutions for an equivalent rough surface and with numerical simulations.

## 2. Theoretical model

Consider the space and time averaged momentum equation for an incompressible fluid (see e.g. Finnigan 2000)

$$\frac{\partial U_i}{\partial t} + U_j \frac{\partial U_i}{\partial x_j} = -\frac{\partial p}{\partial x_i} + \frac{\partial \tau_{ij}}{\partial x_j} - ca|\mathbf{U}|U_i. \quad (1)$$

where  $U_i$  are the velocity components,  $p$  is the pressure field,  $\tau_{ij}$  are the stress tensor components. The last term represents the drag due to the canopy where  $c$  is the drag coefficient and  $a$  is the canopy density. Outside the canopy this term is zero.

Here we assume a forest canopy with a mean canopy density  $a_0$  and sinusoidal variations about this mean. The canopy depth,  $h$ , and the drag coefficient,  $c$ , are kept constant. The variations have wavelength  $4L$  (by analogy with the definition of  $L$  in FB), so the wavenumber is given by  $k = \pi/(2L)$ . The perturbed canopy density is given by

$$a = a_0(1 + \eta e^{ikx}) \quad (2)$$

where the parameter  $\eta$  determines the magnitude of the variations in canopy density and is assumed small.

Assuming a mixing-length model with constant mixing length in the canopy, the background flow (for constant

canopy density  $a_0$ ) can be derived as (see e.g. FB)

$$U_B = \begin{cases} U_h e^{\beta z/l_0} & z < 0 \\ \frac{u_*}{\kappa} \ln\left(\frac{z+d_0}{z_0}\right) & z \geq 0 \end{cases} \quad (3)$$

where  $l_0 = 2\beta^3 L_c$  is the canopy mixing length,  $L_c = 1/(ca_0)$  is the canopy adjustment length (see Coceal and Belcher 2004) and  $\beta$  is an empirical constant. The velocity scale  $U_h$  is the velocity at canopy top,  $u_*$  is the friction velocity at canopy top,  $z_0$  is the canopy roughness length,  $d_0$  is the canopy displacement height and  $\kappa$  is von Karman's constant. The vertical coordinate,  $z$ , is defined so  $z = 0$  is the canopy top. Matching solutions at canopy top (see e.g. FB) gives

$$\begin{aligned} \beta &= u_*/U_h, & U_h &= \frac{u_*}{\kappa} \ln\left(\frac{d_0}{z_0}\right), \\ d_0 &= l_0/\kappa, & z_0 &= \frac{l_0}{\kappa} e^{-\kappa/\beta}. \end{aligned} \quad (4)$$

Physical we imagine that increasing (decreasing) the canopy density from its mean value will increase (decrease) the drag and decelerate (accelerate) the horizontal flow. This in turn will lead to convergence (divergence) in the horizontal flow, and hence through continuity will generate a positive (negative) vertical velocity in the canopy. It is this process, and the impact of this induced motion on the larger scale flow, that we wish to investigate.

As in BXH, solutions within and above a canopy of variable density can be written as

$$\begin{aligned} u &= U_B(z) + \Delta\tilde{u}(x, z), & w &= \Delta\tilde{w}(x, z), \\ p &= P_B + \Delta\tilde{p}(x, z), & \tau &= \tau_B + \Delta\tilde{\tau}(x, z), \\ \tau_{zz} &= \tau_{zzB} + \Delta\tilde{\tau}_{zz}(x, z), \end{aligned} \quad (5)$$

for the streamwise velocity, vertical velocity, kinematic pressure, kinematic turbulent shear stress and  $z$  component normal stress respectively. The subscript  $B$  denotes background solutions and  $\Delta$  a perturbation about that background state. Again following BXH,  $U_0$  (the velocity

scale in the outer region) is a sensible scaling for all velocities, except for the shear stress term which is scaled on  $\rho u_*^2$ . The scaling arguments given in BXH for the perturbations are followed here, but with the forcing parameter,  $\eta$ , which controls the variations in canopy density replacing the parameter  $M$  which controls the variations in surface roughness in BXH. This leads to

$$\begin{aligned} U_B &= U_0 U, & \Delta u &= U_0 \frac{\epsilon \eta}{\kappa} \tilde{u}, & \Delta w &= U_0 \frac{\epsilon \eta}{\kappa} \tilde{w}, \\ \Delta p &= \rho U_0^2 \frac{\epsilon \eta}{\kappa} \tilde{p}, & \Delta \tau &= \rho u_*^2 \frac{\epsilon \eta}{\kappa} \tilde{\tau}, & \Delta \tau_{xx} &= \rho u_*^2 \frac{\epsilon \eta}{\kappa} \tilde{\tau}_{xx}, \\ \Delta \tau_{zz} &= \rho u_*^2 \frac{\epsilon \eta}{\kappa} \tilde{\tau}_{zz} \end{aligned} \quad (6)$$

where  $\epsilon = u_*/U_0$  is the small parameter in the expansion of the solution away from the canopy. For small variations in canopy density ( $\eta \ll 1$ ) the perturbations are small enough that the equations of motion can be linearized about the basic state. The horizontal and vertical momentum equations and the continuity equation then become (to  $O(\eta)$ )

$$U \frac{\partial \tilde{u}}{\partial x} + \tilde{w} \frac{\partial U}{\partial z} = -\frac{\partial \tilde{p}}{\partial x} + \epsilon^2 \left( \frac{\partial \tilde{\tau}_{xx}}{\partial x} + \frac{\partial \tilde{\tau}}{\partial z} \right) - (1 - H(z)) \left( \frac{2U\tilde{u}}{L_c} + \frac{\kappa U^2 e^{ikx}}{\epsilon L_c} \right) \quad (7)$$

$$U \frac{\partial \tilde{w}}{\partial x} = -\frac{\partial \tilde{p}}{\partial z} + \epsilon^2 \left( \frac{\partial \tilde{\tau}}{\partial x} + \frac{\partial \tilde{\tau}_{zz}}{\partial z} \right) - (1 - H(z)) \frac{U\tilde{w}}{L_c} \quad (8)$$

$$0 = \frac{\partial \tilde{u}}{\partial x} + \frac{\partial \tilde{w}}{\partial z} \quad (9)$$

where  $H$  is the Heaviside function defined by  $H(z) = 0, z < 0$  and  $H(z) = 1, z > 0$ .

The upper boundary conditions are that the perturbations all decay far above the canopy so

$$\tilde{u}, \tilde{w}, \tilde{p}, \tilde{\tau} \rightarrow 0 \text{ as } z/L \rightarrow \infty. \quad (10)$$

At the top of the canopy the velocity and turbulent stress are continuous. The mixing length is also assumed continuous, and so continuity of stress implies that the velocity gradient

is continuous at canopy top. At the lower boundary at the bottom of the canopy a free-slip boundary condition is used so  $\tilde{w} = 0$  at  $z = -h$ . It is also assumed that the canopy is deep enough that all the momentum is absorbed by the canopy so  $U_B \rightarrow 0$  and  $\tau \rightarrow 0$  as  $z \rightarrow -h$ , i.e.  $\exp(-\beta h/l_0) \ll 1$ .

To develop the solution consider a single Fourier mode with wavelength  $k$  so  $\tilde{X} = X e^{ikx}$  for any quantity  $X$ .

For the shear stress term, the mixing length model gives

$$\tau = l_m^2 \left( \frac{\partial U}{\partial z} \right)^2 \quad (11)$$

to  $O(\eta^2)$ . The mixing length,  $l_m$  is given by

$$l_m = \begin{cases} l & z < 0 \\ \kappa(z+d) & z \geq 0. \end{cases} \quad (12)$$

Assuming that the local turbulence is always in equilibrium with the change in canopy density then

$$l = l_0/(1 + \eta e^{ikx}) = l_0(1 - \eta e^{ikx} + O(\eta^2)) \quad (13)$$

and

$$d = d_0/(1 + \eta e^{ikx}) = d_0(1 - \eta e^{ikx} + O(\eta^2)). \quad (14)$$

The shear stress term  $\tau$  is then linearized as

$$\tau = \begin{cases} 2\kappa\epsilon^{-1} e^{\beta z/l_0} \left( d_0 \frac{\partial u}{\partial z} - e^{\beta z/l_0} \right) & z < 0 \\ 2\kappa\epsilon^{-1} \left( (z+d_0) \frac{\partial u}{\partial z} - \frac{d_0}{z+d_0} \right) & z \geq 0. \end{cases} \quad (15)$$

Following Belcher *et al.* (1993) and BXH the perturbations in  $\tau_{xx}$  and  $\tau_{zz}$  are modelled as  $\tau_{xx} = \alpha_1 \tau$  and  $\tau_{zz} = \alpha_3 \tau$ , where the constants  $\alpha_1 = 6.3$  and  $\alpha_3 = 1.7$  are taken from BXH and were originally derived from observations in the atmospheric boundary layer. These are not important at leading order, but are required for the higher order terms in the solution.

So far this is very similar to the analysis of FB for flow over a hill (apart from the additional term in Eq. 7 due

to the variations in canopy density) and to the analysis of BXH for flow over a surface of variable roughness (with the addition of the canopy). The difference from the analysis of FB is that rather than being caused by the vertical velocities generated as the air flows over the hill, in this case the pressure field is generated by the (generally smaller) vertical velocities due to the horizontal canopy flow being slowed down or accelerated as the canopy drag increases or decreases.

## 2.1. Flow within the canopy

### 2.1.1. Upper canopy solution

As in FB, the pressure within the inner layer and in the canopy is, to leading order, constant with height so  $p = p_0(x)$ . This follows from analysis of the vertical momentum equation, Eq. (8), and the fact that the canopy depth and inner layer depth are both small compared to the horizontal lengthscale,  $L$ , of the canopy variations. Comparing the advection and drag terms in the canopy gives

$$\frac{U_B \partial u / \partial x}{2U_B u / L_c} \sim \frac{U_h k u}{2U_h u / L_c} \sim \frac{k L_c}{2} \ll 1 \quad (16)$$

which shows that advection is small in the canopy compared to the drag term provided the canopy adjustment lengthscale  $L_c$  is small compared to the lengthscale over which the canopy density varies. The pressure field is a response to the induced vertical velocity in the flow rather than a leading order forcing, and so the pressure gradient term might also be expected to be small. In the upper canopy this may be true. While the velocity and shear stress perturbations decay deep within the canopy, the pressure gradient remains constant and so, provided the canopy is sufficiently deep, the pressure gradient must become important at some point. For this reason the pressure gradient is retained.

Therefore, to leading order, the perturbations in the shear stress gradient, pressure gradient and drag are important

and, on substituting the expression for  $\tau$ , Eq. (7) becomes

$$i\beta kL_c p_0 e^{-Z} = u'' + u' - 2u - 3\frac{\kappa}{\beta} e^Z \quad (17)$$

where the vertical coordinate is transformed to  $Z = \beta z/l_0$  and a prime denotes differentiation with respect to  $Z$ . The general solution to this differential equation is

$$u = \frac{\kappa}{\beta} Z e^Z - \frac{1}{2} i k L_c p_0 e^{-Z} + A e^Z + B e^{-2Z} \quad (18)$$

where the last 2 terms are the solutions of the homogeneous equation and  $A$  and  $B$  are complex constants to be determined from the boundary conditions at the top and bottom of the canopy. Using Eqs. 15 and 18 the shear stress perturbation is

$$\tau = 2\beta\epsilon^{-1} \left( \frac{\kappa}{\beta} Z e^{2Z} + \frac{1}{2} i k L_c p_0 + A e^{2Z} - 2B e^{-Z} \right). \quad (19)$$

Physically the shear stress cannot grow exponentially deep in the canopy and so  $B = 0$ . The same assumption is made in FB. Substituting Eq. (18) into the continuity equation, Eq. (9), and integrating (using the kinematic boundary condition  $w = 0$  at  $z = -h$ ) gives the canopy vertical velocity as

$$w = -2\beta^2 i k L_c \left( \frac{\kappa}{\beta} (Z - 1) e^Z + (1 + \beta h/l_0) e^{-\beta h/l_0} + \frac{1}{2} i k L_c p_0 (e^{-Z} - e^{\beta h/l_0}) + A (e^Z - e^{-\beta h/l_0}) \right). \quad (20)$$

As hypothesised, the pressure gradient term increases exponentially in the canopy in the expression for  $u$  while the other terms decay exponentially and so it will always become important in a sufficiently deep canopy.

Note that the term involving  $p_0$  in  $u$  increases exponentially with depth in the canopy, while the background flow decays exponentially, and so for a sufficiently deep canopy the linearization assumption that  $\Delta u \ll U_B$  will fail. Unlike the problem of flow over a forested hill studied by FB, the pressure here is not a

leading order driver of the flow, but a response to the flow caused by variations in canopy density, and therefore is much smaller. One consequence of this is that the canopy needs to be much deeper before the non-linearity becomes important. Comparing the term in  $u$  which contains the pressure gradient and the background flow gives

$$\frac{\Delta u}{U_B} \sim \eta \frac{\beta}{2\kappa} k L_c p_0 \exp(-2Z) \quad (21)$$

and so the condition for the linearization to be valid throughout the canopy is that

$$\frac{\beta}{2\kappa} \eta k L_c p_0 \exp(2\beta h/l_0) \ll 1. \quad (22)$$

This condition is not automatically satisfied. Although  $\eta$ ,  $kL_c$  and  $p_0$  are all small, the exponential term is large (since  $\exp(-\beta h/l_0) \ll 1$ ) and so for a sufficiently deep canopy it will dominate.

### 2.1.2. Deep canopy solution

If the canopy is sufficiently deep that the canopy solution becomes non-linear then Eqs. (18) and (19) are still valid in the upper canopy. Deep in the canopy the solution becomes non-linear because the linearization of the drag term fails. In this deep canopy limit the stress perturbation,  $\tau$ , becomes independent of  $z$  and so, as in the solution of FB, the dominant balance is now between the unbalanced part of the drag term and the pressure gradient so

$$-\frac{dp_0}{dx} = \frac{U|U|}{L_c} - \frac{U_B^2}{L_c} \quad (23)$$

which is an algebraic equation with solution

$$U = |U_B^2 - L_c dp_0/dx|^{1/2} \operatorname{sgn}(U_B^2 - L_c dp_0/dx) \quad (24)$$

where  $U$  is the full (dimensional) horizontal velocity  $U = U_B + \Delta \tilde{u}$ . As acknowledged by FB this equation is heuristic, however the assumptions made in deriving it are physically reasonable and it agrees well with numerical

simulations (e.g. Ross and Vosper 2005). Unlike the solution of FB over a hill, the  $p_0$  in this expression is the second order pressure induced by the canopy flow rather than the leading order pressure perturbation generated by the inviscid flow over the hill. This deep canopy solution can be approximated as

$$U = U_B - \frac{1}{2} \frac{L_c dp_0/dx}{U_h} \exp(-Z) \quad (25)$$

towards the upper part of the canopy. This form matches with the upper canopy solution Eq. (18) in the limit  $Z \rightarrow -\infty$  in the upper canopy solution. One important consequence of this deep canopy solution is that flow may become reversed ( $U < 0$ ) deep in the canopy if the pressure gradient is large enough, or the canopy is deep enough (i.e.  $U_B$  is small enough), whereas the linear solution always remains positive since the  $u$  perturbations must remain smaller than the background velocity  $U_B$ .

In the same way as described in FB, a uniformly valid solution throughout the canopy may be derived by combining the deep canopy solution with the parts of the upper canopy solution not involving the pressure term to give

$$U = |U_B^2 - L_c dp_0/dx|^{1/2} \operatorname{sgn}(U_B^2 - L_c dp_0/dx) + U_0 \frac{\epsilon \eta}{\kappa} \left( \frac{\kappa}{\beta} Z e^Z + A e^Z \right) \exp(ikx) \quad (26)$$

in dimensional form. This form agrees asymptotically with both the upper and lower canopy solutions and provides a convenient expression which may be applied throughout the canopy.

In order to calculate the pressure field in the following sections it is necessary to obtain the canopy-top vertical velocity field. This can be done using the uniformly valid canopy solution for  $U$  given in Eq. (26), either by integrating the continuity equation or by calculating the streamfunction of the flow. In order to do this it is convenient to split  $U$  into two parts - the linear upper canopy

part and the non-linear deep canopy part, as done in FB. This gives

$$U_u = U_0 \frac{\epsilon \eta}{\kappa} \left( \frac{\kappa}{\beta} Z e^Z + A e^Z \right) \exp(ikx) \quad (27)$$

$$U_d = |U_B^2 - L_c dp_0/dx|^{1/2} \operatorname{sgn}(U_B^2 - L_c dp_0/dx). \quad (28)$$

The linear part coming from the upper canopy solution is easily integrated to give a vertical velocity

$$w_u = -U_0 \frac{\epsilon \eta}{\kappa} 2\beta^2 ik L_c \exp(ikx) \left( \frac{\kappa}{\beta} (Z-1) e^Z + \frac{\kappa}{\beta} \left( 1 + \frac{\beta h}{l_0} \right) e^{-\beta h/l_0} + A \left( e^Z - e^{-\beta h/l_0} \right) \right). \quad (29)$$

The non-linear, deep-canopy, part has to be integrated by dividing the canopy up into different regions depending on the sign of the terms. This non-linear part is however identical in form to the non-linear component of the canopy flow in FB. The only differences are in the source and magnitude of the pressure field  $p_0$ . In particular over a variable density canopy it is not known a priori where the pressure gradient will be zero, or where the term  $U_B^2 - L_c dp_0/dx$  will be zero. The solution for  $w_d$  in this case is therefore the same as in FB, but with a phase shift depending on the phase of  $p_0$ . For completeness these solutions are given in Appendix A.

## 2.2. Flow above the canopy

The flow above the canopy is divided into 2 regions, the inner region where the Reynolds stresses are important and the outer region where the flow is essentially inviscid. Hunt *et al.* (1988) estimate the height of the inner region,  $h_i$ , as the solution to the implicit equation

$$kh_i \log(h_i/z_0) = 2\kappa^2. \quad (30)$$

The outer region is further divided into two layers, the middle layer where the curvature of the mean velocity profile is still important (even though the shear stresses

which cause it are negligible) and an outer layer where the flow is potential flow. For a logarithmic wind profile Hunt *et al.* (1988) give the height of the middle layer,  $h_m$ , as the solution to the implicit equation

$$h_m \log^{1/2}(h_m/z_0) = L. \quad (31)$$

In the solution of BXH for flow over a surface of variable roughness the inner region is divided in two layers. The shear stress layer (SSL) where Reynolds stress terms are important makes up most of the inner region. Near the surface is the thin inner surface layer (ISL) over which the SSL solution is matched to the no-slip boundary condition at the surface. The unknown coefficients in the solutions are determined by asymptotically matching the solutions between the different layers.

The solution method above the canopy is essentially the same as that of BXH with the important difference that the SSL solution is directly matched to the canopy solution at the canopy top, without the requirement for the ISL. The same procedure is adopted in FB for flow over a canopy-covered hill. While the solution procedure is the same as BXH the matching coefficients take different (complex) values due to the different matching procedure at the bottom of the SSL.

The solutions for flow above the canopy are given below. Details on the derivation can be found in BXH. Note that some of the notation has been changed slightly for consistency with that used here.

### 2.2.1. Shear stress layer

In the shear stress layer above the canopy then (following BXH) the flow variables are scaled as

$$u = \hat{u}, \quad w = \hat{w}, \quad \tau = \frac{2}{U(h_i)} \hat{\tau}, \quad p = -U(h_i) \hat{p} \quad (32)$$

where  $h_i$  is the inner layer height. The scaled vertical coordinate in the SSL is  $\zeta = (z + d)/h_i$ . On substituting

these scaled variables the linearized equations become

$$\begin{aligned} (1 + \delta \ln \zeta) i \hat{u} + \frac{\hat{w}}{2\kappa^2 \zeta} &= i p + \frac{\partial}{\partial \zeta} \left( \zeta \frac{\partial \hat{u}}{\partial \zeta} - \frac{\zeta_0}{\zeta} \right) \\ &\quad - 2\delta i \kappa^2 \alpha_1 \left( \zeta \frac{\partial \hat{u}}{\partial \zeta} - \frac{\zeta_0}{\zeta} \right) \\ 2\kappa^2 \delta (1 + \delta \ln \zeta) i \hat{w} &= \frac{\partial \hat{p}}{\partial \zeta} + 4\kappa^4 i \delta^2 \left( \zeta \frac{\partial \hat{u}}{\partial \zeta} - \frac{\zeta_0}{\zeta} \right) \\ &\quad - 2\delta \kappa^2 \alpha_3 \frac{\partial}{\partial \zeta} \left( \zeta \frac{\partial \hat{u}}{\partial \zeta} - \frac{\zeta_0}{\zeta} \right) \\ \hat{w} &= -2i \kappa^2 \delta \int_{\zeta_0}^{\zeta} \hat{u}(\zeta') d\zeta' + \hat{w}_c \\ \hat{\tau} &= \frac{1}{\delta} \left( \zeta \frac{\partial \hat{u}}{\partial \zeta} - \frac{\zeta_0}{\zeta} \right) \end{aligned} \quad (33)$$

where  $\zeta_0 = d_0/h_i$  and  $\delta = \log^{-1}(h_i/z_0)$  is the small parameter in this region. The canopy top vertical velocity is given by  $\hat{w}_c$ . Solutions for the flow variables are expanded in powers of  $\delta$  so, for example,  $\hat{u} = u^{(0)} + \delta u^{(1)} + O(\delta^2)$ .

In order to match the canopy solution to this SSL expansion it is useful to note that  $kL_c$ , which appears in the canopy solutions, can be written as  $kL_c = \delta 2\kappa^2 L_c/h_i$ . This means that  $\hat{w}_c$  is  $O(\delta)$  and so  $w^{(0)} = 0$  from the integrated continuity equation. Since the pressure field is induced in response to the vertical velocity at canopy top then again the leading order pressure field is zero,  $p^{(0)} = 0$ . Using these leading order terms the horizontal momentum equation reduces to

$$\frac{\partial}{\partial \zeta} \left( \zeta \frac{\partial u^{(0)}}{\partial \zeta} \right) - i u^{(0)} = -\frac{\zeta_0}{\zeta^2}. \quad (34)$$

In order for  $u^{(0)}$  to remain bounded as  $\zeta \rightarrow \infty$  the homogeneous solution of this equation must be of the form  $A_0 K_0[2(i\zeta)^{1/2}]$  where  $A_0$  is the constant of integration (a matching coefficient to be determined by matching the solution to the layers above and below) and  $K_0$  is the modified Bessel function of zeroth order (as in BXH). A solution to the inhomogeneous equation can be found by transforming Eq. (34) using the substitutions  $s = 2e^{3i\pi/4} \zeta^{1/2}$  and  $u = 16i\zeta_0 v$  to give the Lommel differential equation

$$v'' + \frac{1}{s} v' + v = s^{-4} \quad (35)$$

which has a solution  $S_{-3,0}$  (Olver *et al.* 2010) where  $S_{-3,0}$  is a Lommel function. Note that this form of the equation could be used to write the general solution in terms of Bessel functions rather than modified Bessel functions, but for consistency with previous work, modified Bessel functions are used. The solution for  $u^{(0)}$  is then

$$u^{(0)} = A_0 K_0(2e^{i\pi/4}\zeta^{1/2}) + 16i\zeta_0 S_{-3,0}(2e^{3i\pi/4}\zeta^{1/2}). \quad (36)$$

At  $O(\delta)$  the continuity equation gives

$$\begin{aligned} w^{(1)} &= -2\kappa^2 \int_{\zeta_0}^{\zeta} iu^{(0)}(\zeta') d\zeta' = -2\kappa^2 \left[ \zeta \frac{\partial u^{(0)}}{\partial \zeta} - \frac{\zeta_0}{\zeta} \right]_{\zeta_0}^{\zeta} \\ &= w_c^{(1)} - 2\kappa^2 \left[ A_0 \left( \zeta \frac{\partial K_0}{\partial \zeta} - \zeta_0 K'_{00} \right) \right. \\ &\quad \left. + 16i\zeta_0 \left( \zeta \frac{\partial S_{-3,0}}{\partial \zeta} - \zeta_0 S'_{00} \right) + (1 - \zeta_0/\zeta) \right] \end{aligned} \quad (37)$$

where

$$K'_{00} = \left. \frac{\partial K_0[2(i\zeta)^{1/2}]}{\partial \zeta} \right|_{\zeta=\zeta_0 \equiv d_0/h_i}, \quad (38)$$

$$S'_{00} = \left. \frac{\partial S_{-3,0}[2e^{3i\pi/4}\zeta^{1/2}]}{\partial \zeta} \right|_{\zeta=\zeta_0 \equiv d_0/h_i} \quad (39)$$

and  $w_c^{(1)}$  is the  $O(\delta)$  canopy top vertical velocity.

The vertical momentum equation at  $O(\delta)$  is

$$\frac{\partial p^{(1)}}{\partial \zeta} = -2\kappa^2 \frac{\partial \tau_{33}}{\partial \zeta} = 2\kappa^2 \alpha_3 \frac{\partial}{\partial \zeta} \left( \zeta \frac{\partial u^{(0)}}{\partial \zeta} - \frac{\zeta_0}{\zeta} \right). \quad (40)$$

Integrating and matching with the leading order pressure perturbation  $\sigma^{(1)}(k, 0)$  at canopy top ( $z = 0$ ,  $\zeta = d/h_i = \zeta_0$ ) gives

$$\begin{aligned} p^{(1)} &= \sigma^{(1)} + 2\kappa^2 \alpha_3 \left[ A_0 \left( \zeta \frac{\partial K_0}{\partial \zeta} - \zeta_0 K'_{00} \right) \right. \\ &\quad \left. + 16i\zeta_0 \left( \zeta \frac{\partial S_{-3,0}}{\partial \zeta} - \zeta_0 S'_{00} \right) + 1 - \frac{\zeta_0}{\zeta} \right]. \end{aligned} \quad (41)$$

The pressure is small (i.e.  $p_0 = O(\delta)$ ) and therefore the  $p_0$  term is not significant in the expression for  $u$  in the upper canopy. This means that to leading order the matching

coefficients  $A$  and  $A_0$  can be found without requiring a full solution in the middle and outer layers. Matching  $u$  and  $\tau$  at canopy top gives a pair of linear simultaneous equations for  $A$  and  $A_0$  which can be solved giving

$$A_0 = \frac{1 - 16i\zeta_0 \left( \zeta_0 S'_{00} - \frac{\beta}{\kappa} S_{00} \right)}{\zeta_0 K'_{00} - \frac{\beta}{\kappa} K_{00}}, \quad (42)$$

$$A = \frac{K_{00} + 16i\zeta_0^2 (S_{00} K'_{00} - K_{00} S'_{00})}{\zeta_0 K'_{00} - \frac{\beta}{\kappa} K_{00}}. \quad (43)$$

In order to match with the middle layer solution the expressions for  $w$  and  $p$  must be evaluated in the limit  $\zeta \rightarrow \infty$ . Noting that  $K_0$ ,  $\zeta \partial K_0 / \partial \zeta$ ,  $S_{-3,0}$  and  $\zeta \partial S_{-3,0} / \partial \zeta \rightarrow 0$  in this limit we obtain

$$\begin{aligned} w &\sim \left\{ \delta(2\kappa^2 (A_0 \zeta_0 K'_{00} + 16i\zeta_0^2 S'_{00} - 1) + w_c^{(1)}) + O(\delta^3) \right\} \\ p &\sim -U(h_i) \left\{ \delta(\sigma^{(1)} - 2\alpha_3 \kappa^2 (A_0 \zeta_0 K'_{00} + 16i\zeta_0^2 S'_{00} - 1)) \right. \\ &\quad \left. + O(\delta^3) \right\}. \end{aligned} \quad (44)$$

### 2.2.2. Middle layer

In the middle layer solution the Reynolds stress terms are negligible at leading order and the effect of the background velocity gradient dominates over the streamwise acceleration so the equations of motion reduce to the single equation

$$\frac{\partial^2 w}{\partial z^2} - \frac{U''}{U} w = 0 \quad (45)$$

for  $w$ . The general solution of this (see BXH) is

$$w^{(0)} = B_0 U + C_0 U \int_{\hat{z}}^{\hat{z}'} \frac{d\hat{z}'}{U^2(\hat{z}' h_m)} \quad (46)$$

where  $\hat{z} = z/h_m$  and  $h_m$  is the middle layer height. Substituting this expression for  $w^{(0)}$  into the continuity equation gives

$$u^{(0)} = -\frac{1}{ikh_m} \left[ B_0 U' + \frac{C_0}{U} \left( 1 + U U' \int_{\hat{z}}^{\hat{z}'} \frac{d\hat{z}'}{U^2(\hat{z}' h_m)} \right) \right]. \quad (47)$$

The vertical momentum equation shows that at leading order the pressure is constant. Matching these solutions to the SSL solutions for  $w$  and  $p$  at large  $\zeta$  proceeds just as in BXH and gives

$$B_0 = \frac{(2\kappa^2(A_0\zeta_0 K'_{00} + 16i\zeta_0^2 S'_{00} - 1) + w_c^{(1)})}{U(h_i)} \delta \quad (48)$$

$$C_0 = -ikh_m \delta U(h_i) (\sigma^{(1)} - 2\alpha_3 \kappa^2 (A_0 \zeta_0 K'_{00} + 16i\zeta_0^2 S'_{00} - 1)). \quad (49)$$

For large  $z$  these solutions asymptote to

$$u \sim \delta U(h_i) \left\{ (\sigma^{(1)} - 2\alpha_3 \kappa^2 (A_0 \zeta_0 K'_{00} + 16i\zeta_0^2 S'_{00} - 1)) + O(h_m k) \right\} \quad (50)$$

$$w \sim \delta \left\{ \frac{(2\kappa^2(A_0\zeta_0 K'_{00} + 16i\zeta_0^2 S'_{00} - 1) + w_c^{(1)})}{U(h_i)} + O(h_m k) \right\}. \quad (51)$$

Again the form of this solution is identical to that of BXH, the difference lies in the values of the constants.

### 2.2.3. Upper layer

In the upper layer shear in the background flow is negligible and the problem reduces to potential flow,

$$\frac{\partial^2 w}{\partial x^2} + \frac{\partial^2 w}{\partial z^2} = 0, \quad (52)$$

at leading order which has the solution (see BXH)

$$\begin{aligned} w^{(0)} &= D_0 e^{-kz} \\ u^{(0)} &= -iD_0 e^{-kz} = -p^{(0)}. \end{aligned} \quad (53)$$

Matching these to the middle layer solutions gives

$$D_0 = \frac{\delta(2\kappa^2(A_0\zeta_0 K'_{00} + 16i\zeta_0^2 S'_{00} - 1) + w_c^{(1)})}{U(h_i)} \quad (54)$$

$$\begin{aligned} \sigma^{(1)} &= 2\kappa^2(A_0\zeta_0 K'_{00} + 16i\zeta_0^2 S'_{00} - 1) \left( \alpha_3 - \frac{i}{U(h_i)^2} \right) \\ &\quad - \frac{iw_c^{(1)}}{U(h_i)^2}. \end{aligned} \quad (55)$$

Assuming that the canopy top vertical velocity is dominated by the linear upper canopy solution then  $w_c^{(1)}$  can be obtained from Eq. (29).

### 3. Validity of solution

In deriving the analytical solution a number of assumptions are made. Firstly we assume that the canopy is sufficiently deep that the momentum is predominantly absorbed in the canopy rather than at the surface, i.e.  $\exp(\beta h/l_0) \gg 1$ . Secondly we assume that variations in the canopy density are small,  $\eta \ll 1$ , so that the equations of motion can be linearized. Thirdly we assume that advection in the canopy is small compared to the perturbation drag term, which requires  $kL_c \ll 1$ . Finally, in deriving the equations of motion for canopy flow in the form presented here it is necessary to perform volume averaging over a number of obstacles in order to obtain smooth and well defined canopy drag and turbulence terms (see e.g. Finnigan 2000). For homogeneous canopies and flows this does not present a problem, but for inhomogeneous problems the averaging lengthscale should be considered. For this problem to be well defined it is therefore required that the canopy adjustment lengthscale,  $L_c$ , and the lengthscale over which the canopy density varies,  $L$ , are larger than the averaging lengthscale,  $L_{av}$ . For a dense forest canopy then  $L_{av}$  might be of the order of a few metres with  $L_c$  being perhaps of order 10 m and so this is a reasonable assumption. The analytical solution already requires  $kL_c \ll 1$  and so the condition that  $L \gg L_{av}$  is also satisfied. For forest canopies the precise ratio of  $L_c$  to  $L_{av}$  will depend on the species,

maturity and initial spacing of the trees, but the assumptions made here are likely to remain valid.

In deriving the solution we also assume that in the upper canopy the horizontal pressure gradient term is not significant. This means that the leading order balance is between the drag and the stress terms. The drag term changes both because of the density changes and because of changes in the flow speed. This is balanced by the changes in the stress term due to the changing flow. For the pressure gradient to be negligible near canopy top requires

$$\frac{dp_0/dx}{2U_B u/L_c} \sim \frac{k\delta U(h_i)A_0}{U_h A/L_c} \sim kL_c \ll 1$$

(where  $w_c^{(1)} \leq 1$  is assumed) which is already satisfied. Formally this means that the pressure gradient and the advection terms are of the same order of magnitude near canopy top, and so for consistency we should have neglected both in deriving the upper canopy solution. The pressure gradient term was retained to aid matching to the deep canopy solution, but is neglected when matching the canopy solution to the SSL solution above.

To check that  $w_c^{(1)} \leq 1$  it is easiest to consider the upper and deep canopy contributions separately. The upper canopy contribution is

$$w_{uc}^{(1)} \sim 2\beta\kappa kL_c\delta^{-1} \quad (56)$$

using the fact that  $A \rightarrow -\frac{\kappa}{\beta}\delta$  for small  $kL_c$ . Substituting  $\delta = kh_i/(2\kappa^2)$  gives  $w_{uc}^{(1)} \sim 2(\kappa^3/\beta^2)\zeta_0$ . Further note that

$$\begin{aligned} \zeta_0 &= \frac{d_0}{h_i} = \frac{\beta^3}{\kappa^3} kL_c\delta^{-1} \\ &= \frac{\beta^3}{\kappa^3} kL_c \left( \frac{\kappa}{\beta} - \log \zeta_0 \right) \end{aligned} \quad (57)$$

and so  $kL_c \rightarrow 0 \Rightarrow \zeta_0 \rightarrow 0$  and hence  $w_{uc}^{(1)} \rightarrow 0$ . The already assumed condition  $kL_c \ll 1$  is therefore sufficient to ensure that the contribution to the pressure field from the upper canopy part of the vertical velocity is small.

By evaluating  $w_d$  in the limit  $dp_0/dx \rightarrow 0$  and substituting the expression for  $p_0$  one obtains that

$$\begin{aligned} w_{dc}^{(1)} &\sim (kL_c)^2 \beta^2 \frac{p_0}{U_h} \delta^{-1} \exp(\beta h/l_0) \\ &\sim (kL_c)^2 2\beta^3 \kappa \exp(\beta h/l_0). \end{aligned} \quad (58)$$

For the non-linear, deep canopy contribution to the vertical velocity to be negligible in the induced pressure field therefore requires  $(kL_c)^2 \exp(\beta h/l_0) \ll 1$ . This is potentially a more stringent condition than requiring  $(kL_c) \ll 1$  since the exponential term is large and therefore provides an additional requirement for the validity of the analytical solution.

Having derived the pressure field  $p_0$  it is also possible to rewrite the condition for the linear canopy solution to be valid as

$$\beta^2 \eta kL_c \delta \exp(2\beta h/l_0) \ll 1. \quad (59)$$

#### 4. Comparison with numerical results

##### 4.1. Long and short wavelength variations in canopy density

To test the analysis, results are compared with numerical simulations of flow over a flat canopy of uniform height, but varying canopy density using the BLASIUS model. BLASIUS has previously been used for other studies of canopy flow both as a one-and-a-half order mixing length closure model (Ross and Vosper 2005; Ross 2011), and as a large-eddy simulation (LES) model (Ross 2008, 2011). Here the model is run with the one-and-a-half order mixing length closure scheme. The canopy used is similar to that in Ross and Vosper (2005). Details of the parameter values used are given in table I. The canopy density change is sufficiently slow that  $kL_c = 0.0098 \ll 1$  for the long wavelength case ( $L = 1600$  m) and so the advection terms at canopy top are negligible at leading order. For the shorter wavelength simulation ( $L = 100$  m) then  $kL_c = 0.157$  this is not strictly the case. For both cases  $\exp(-\beta h/l_0) = 0.00153$  and so the

Table I. Canopy parameter values from the numerical simulations.

Canopy parameter	Simulation 1	Simulation 2
Canopy height, $h$	10 m	10 m
Drag $c_d$	0.25	0.25
Leaf area density, $a$	$0.4 \text{ m}^{-1}$	$0.4 \text{ m}^{-1}$
Amplitude, $\eta$	$-0.05i$	$-0.05i$
Lengthscale, $L$	1600 m	100 m
Adjustment length, $L_c$	10 m	10 m
Wavelength, $k$	$0.000982 \text{ m}^{-1}$	$0.0157 \text{ m}^{-1}$
Inner layer depth, $h_i$	92.1 m	9.69 m
Middle layer depth, $h_m$	588 m	45.4 m

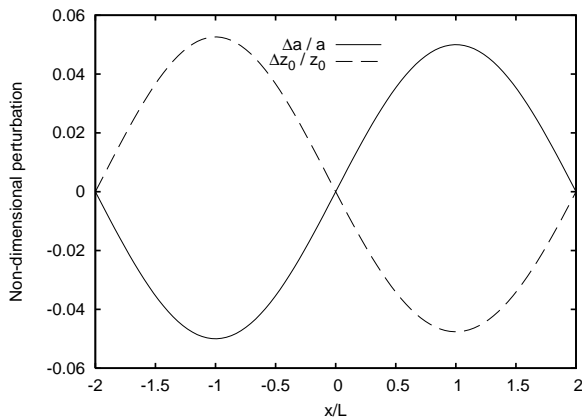


**Figure 1.** Non-dimensional perturbations in the canopy density,  $a$  (solid line) and the roughness length  $z_0$  (dashed line) as a function of horizontal position  $x/L$  for the two simulations presented here.

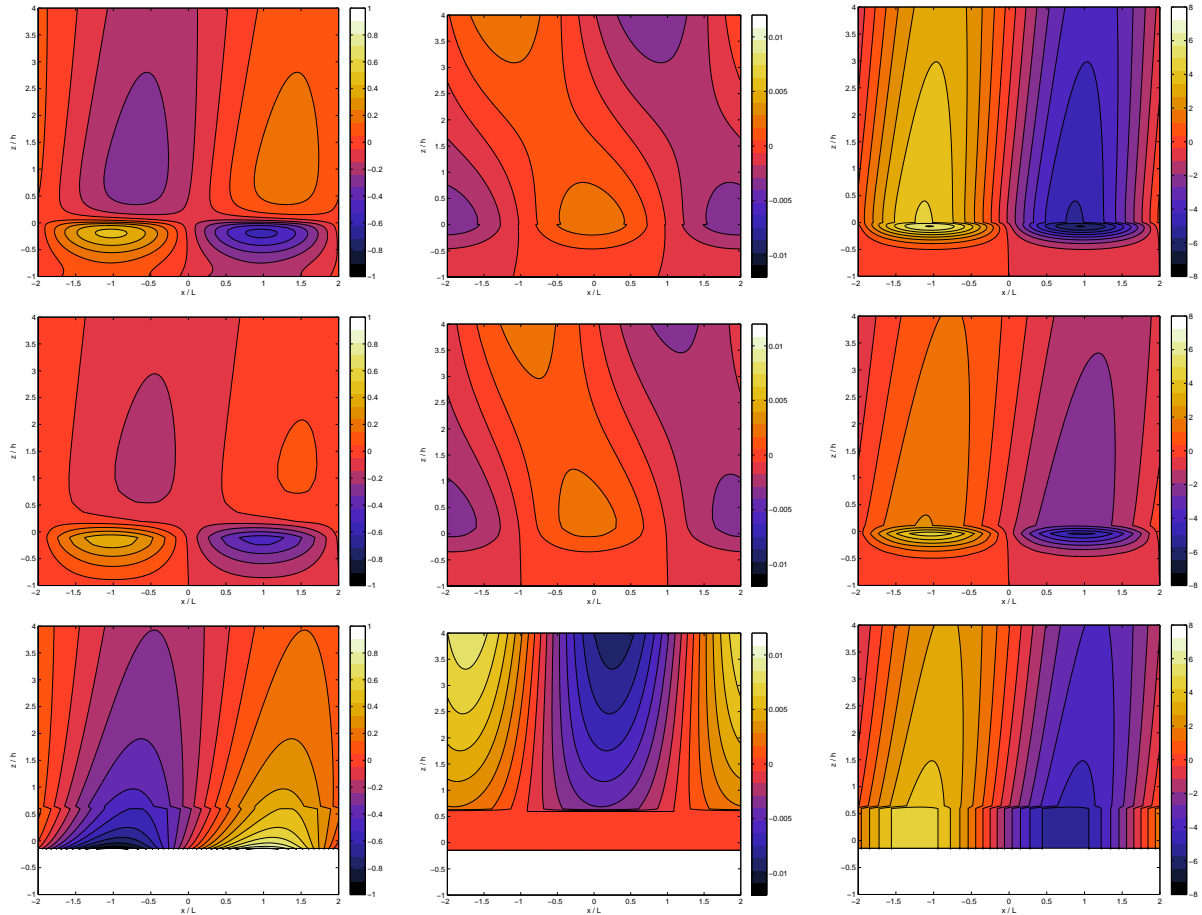
momentum is predominantly absorbed by the canopy. For the long wavelength case this gives  $(kL_c)^2 \exp(\beta h/l_0) = 0.0630$  and so the deep canopy contribution to the vertical velocity is not important in the upper canopy. For the shorter wavelength case  $(kL_c)^2 \exp(\beta h/l_0) = 16.1$  and so the vertical velocity field induced deep in the canopy is likely to be important in the upper canopy solution. Figure 1 shows the non-dimensional canopy density and roughness length perturbations for these cases as a function of the horizontal coordinate  $x/L$ .

Figure 2 shows contour plots of the normalised perturbation horizontal velocity  $u$  and vertical velocity  $w$  for both the analytical solution and the numerical model for the large wavelength ( $L = 1600$  m) case. There is generally good qualitative and quantitative agreement between the model in terms of the magnitude and phase of the induced horizontal and vertical velocity perturbations, although the analytical solution does appear to overestimate the horizontal velocity perturbations compared to the

numerical model, while underestimating the maximum vertical velocities at canopy top. There is some indication of a difference in phase between the vertical velocity in the analytical and numerical models at  $z/h \sim 4$ . This is likely to be related to the turbulence scheme used and is discussed in more detail in the following section. The analytical solution gives strong gradients in the horizontal perturbation at canopy top which are smoothed out in the numerical model, partly due to numerical diffusion and partly due to resolution. Note that although these look large on the contour plots, the actual magnitudes are small compared to the gradients in velocity in the background mean profile since the perturbations are small.

Figure 3 shows similar contour plots of the normalised perturbation horizontal velocity  $u$  and vertical velocity  $w$  for both the analytical solution and the numerical model for the smaller wavelength ( $L = 100$  m) case. Note from table I that in this case the inner layer thickness,  $h_i = 9.69$  m is comparable to the canopy depth and so much of the solution plotted is the middle layer solution.

For the small wavelength case the advection terms at canopy top are no longer negligible at leading order and so the analytical model breaks down. As for flow over a forested hill, reducing the wavelength results in an increased gradient in the horizontal velocity variations (in this case due to a more rapid change in canopy drag rather than a large hill-induced pressure gradient), which in turn increases the vertical velocity induced in the canopy. This is most obviously seen by comparing the vertical velocity in the upper canopy (note the different scales compared to figure 2), which affects the induced pressure field, and leads to the pressure gradient term becoming important in the deep canopy. The canopy-induced shift in the pressure gradient in turn leads to the strong shift in phase of the perturbations in horizontal velocity in the canopy which are observed in the numerical model. The failure of the analytical model to account for the effects of advection and the pressure gradient in the upper canopy mean that the analytical model does not capture these



**Figure 2.** Contour plots of the normalised perturbation horizontal velocity,  $u/(U_0\epsilon\eta/\kappa)$  (left panels) and vertical velocity,  $w/(U_0\epsilon\eta/\kappa)$  (right panels) from the analytical solution (top), numerical model (middle) and the analytical solution of BXH (bottom). Results are shown for the case with  $L = 1600$  m.

phase shifts. The discontinuity in  $w$  at canopy top in the analytical canopy solution is due to the inclusion of the contribution of the pressure gradient term in the canopy vertical velocity expression, while this term is neglected when matching to the SSL vertical velocity above. In the regions of convergence strong vertical velocities are generated for the short wavelength case (figure 3) and this reflects the breakdown of the analytical solution for the short wavelength case.

In both the canopy and roughness length analytical models  $u$  and  $w$  are discontinuous at the inner layer height,  $h_i/h = 0.97$ , because the matching at this interface is asymptotic (see sections 2.2.1 and 2.2.2). Since the definition of the inner layer height is somewhat heuristic and since in reality there is not a sharp interface between the two layers this approach is physically and mathematically reasonable. Blending the two solutions over some range of

heights would produce a smooth solution which might be more realistic and would reflect the fact that physically the transition between these two layers is not abrupt. On the other hand this introduces some arbitrariness in the choice of blending function and disguises the different behaviour of the solutions in the different layers. For this reason no blending has been done in the results presented here. It is worth noting that this asymptotic matching is applied in all the analytical models of this type for flow over hills or heterogeneous terrain (e.g. BXH and FB) but is not widely discussed. For long wavelength variations in terrain or surface properties the inner and middle layer solutions vary relatively smoothly and so the asymptotic matching does not lead to significant discontinuities at the inner layer height (figure 2). As the wavelength of the variations decreases (figure 3) the inner layer solutions change more rapidly with height and so the inner and middle layer

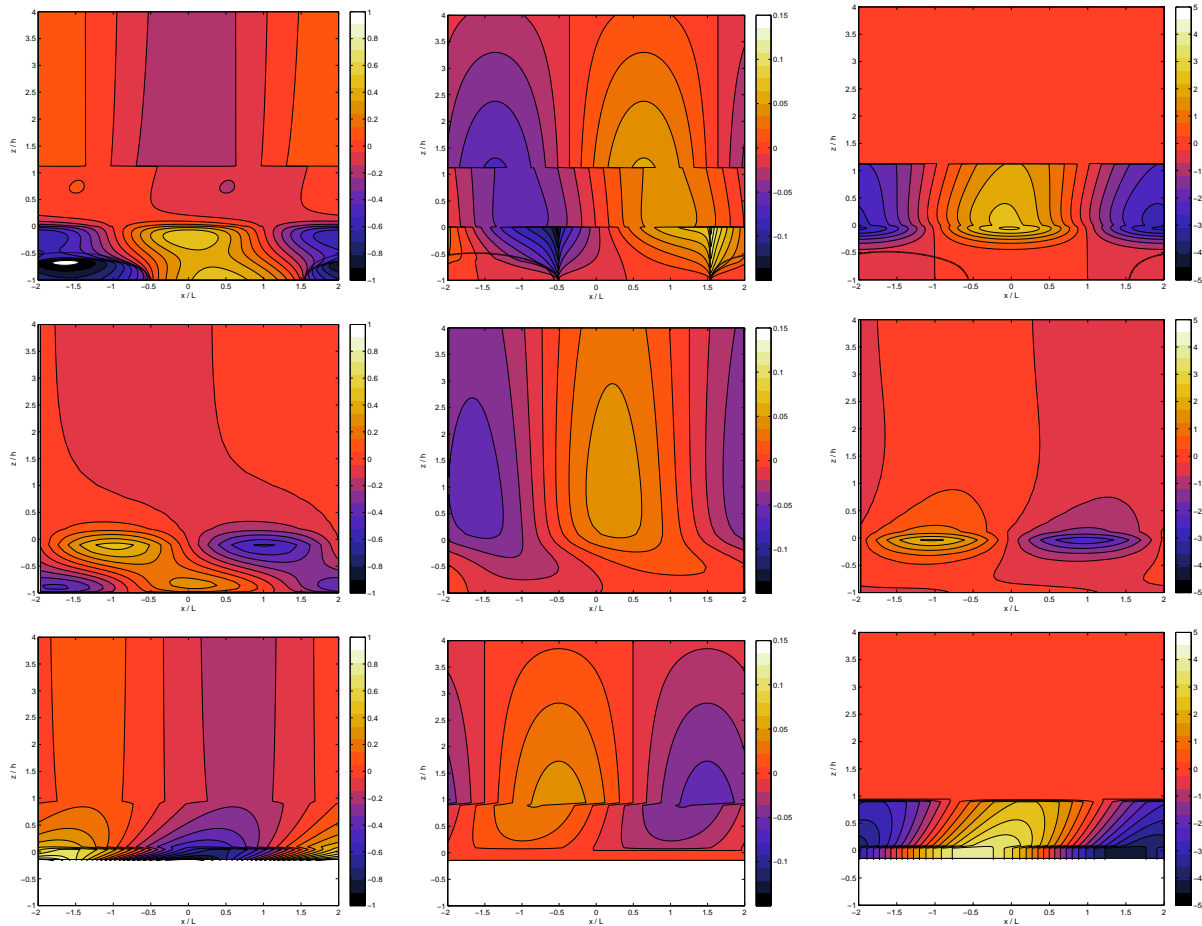


**Figure 3.** Contour plots of the normalised perturbation horizontal velocity,  $u/(U_0\epsilon\eta/\kappa)$  (left panels) and vertical velocity,  $w/(U_0\epsilon\eta/\kappa)$  (right panels) from the analytical solution (top), numerical model (middle) and the analytical solution of BXH (bottom). The thick black line in the top panels marks the recirculation region. Results are shown for the case with  $L = 100$  m.

solution at the inner layer height do not agree so well. This is in part because the inner layer height is less for small wavelengths. For the analytical model developed here the solution breaks down for small wavelengths, including the case shown in figure 3, as the induced vertical velocities in the canopy become sufficiently large that advection terms cannot be neglected. It is therefore perhaps not surprising that the solution is not as well behaved in this case.

Figure 3 is an example where the pressure gradient induced in the canopy is sufficiently large to cause the flow to separate. The streamline delineating the region of separated flow is marked with a thick solid line in figure 3. This can be calculated using the streamfunction given in Appendix A. In this example the recirculation region is relatively shallow. The numerical simulations do not exhibit flow separation, largely because the numerical model has a

no-slip lower boundary condition which tends to reduce the induced flow near the surface and inhibit flow separation.

#### 4.2. Impact of the closure assumptions

The empirical relationship used to parameterize  $\tau_{xx}$  and  $\tau_{zz}$  is worth discussing in further detail. Firstly, the terms involving  $\tau_{xx}$  and  $\tau_{zz}$  are not important in the leading order solutions for the velocity perturbations and so these solutions are relatively insensitive to the turbulence parameterization. Even a mixing length closure scheme will give a reasonably accurate prediction of the shear stress  $\tau$  in the canopy and inner region and therefore get the main induced flow pattern correct. The pressure field in the canopy and inner region comes from the  $\sigma^{(1)}$  term given by Eq. 55 however, which does depend on the  $\tau_{zz}$  term (the solution contains  $\alpha_3$ ) and so will be sensitive to parameterization of this term.

The parameterization used is derived from observations in the free boundary layer. A synthesis of different observations over canopies is given in Finnigan (2000) and shows that both  $\tau_{xx}/\tau$  and  $\tau_{zz}/\tau$  decrease through the roughness sublayer (RSL) above the canopy, with values at canopy top being about 35% smaller than the values above the RSL. The ratios decrease further with depth into the canopy. The parameterization used here does not take into account this variation. Within the canopy the  $\tau_{xx}$  and  $\tau_{zz}$  terms do not appear in the solution presented here and so any decrease with height in the canopy is not important, however in the inner region there is an error in the pressure field associated with the overestimate in  $\tau_{zz}$ .

If instead a mixing length model was used to parameterize  $\tau_{zz}$  so that

$$\tau_{zz} = l_m^2 \frac{dU}{dz} \frac{\partial w}{\partial z} \quad (60)$$

then substitution of the inner layer solutions shows that  $\tau_{zz}/\tau = O(\delta)$  and so can be ignored in the solutions presented here (i.e. setting  $\alpha_3 = 0$ ).

The exact error in the canopy and inner region pressure field resulting from this will depend on the nature of the canopy and its variability. Analysis of Eq. (55) does show that the magnitude of the pressure field will be approximately right if  $\alpha_3$  is set to zero, but there will be a significant shift in the phase of the pressure. Figure 4 show how the analytical canopy pressure field varies for three different values of  $\alpha_3$ , and also the results with the numerical model.

For the longer wavelength variation in canopy drag, the analytical canopy solution with  $\alpha_3 = 0$  (i.e. representing a mixing length scheme) is in very good agreement with the numerical model. Increasing values of  $\alpha_3$  tend to lead to a slight increase in the induced pressure field and a small negative shift in the phase of the surface pressure. These values cover the likely range of values above real canopies based on observations and so give some indication of the uncertainty due to the parameterization of  $\tau_{zz}$ .

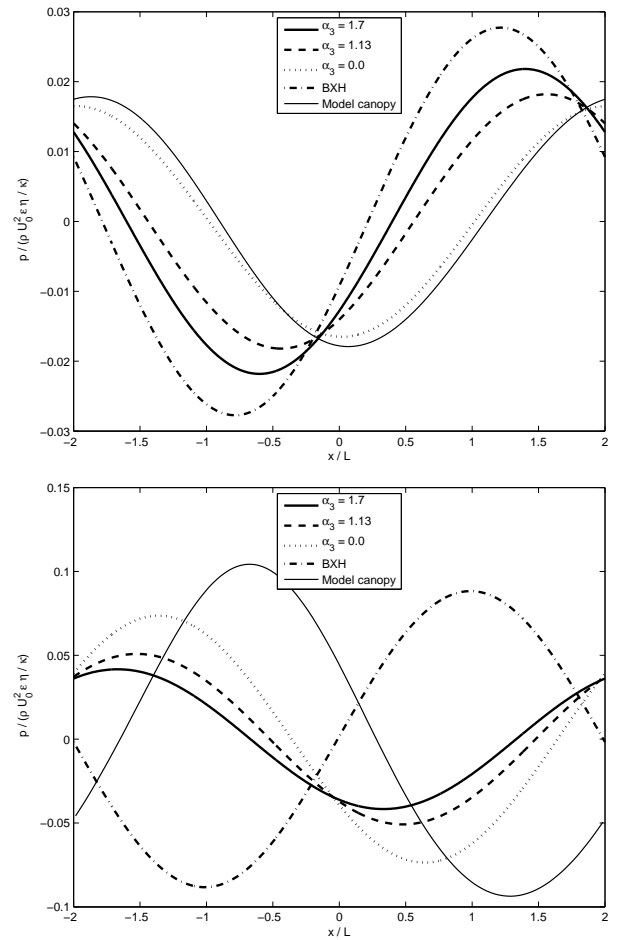


**Figure 4.** Normalised pressure field,  $p/(\rho U_0^2 \epsilon \eta / \kappa)$ , within the canopy as a function of horizontal position. Analytical results using the canopy model are shown for three different values of  $\alpha_3$  along with the analytical results of BXH (with  $\alpha_3 = 1.7$ ) and the numerical results from the mixing length numerical model. Results are for cases with  $L = 1600$  m (top) and  $L = 100$  m (bottom).

For the smaller wavelength variation in canopy drag, where vertical advection at canopy top is no longer negligible, then the pressure field is much larger and predominantly determined by the vertical velocity at canopy top (the  $w_c^{(1)}$  terms in Eq. 55). In this case (bottom plot of figure 4) the variation in the analytical surface pressure field with  $\alpha_3$  is much smaller. There is still a significant phase and amplitude shift between the model and all the analytical canopy solutions, which in this case is due to the analytical model failing to represent the coupling between the canopy and the boundary layer through the advection terms. As in the case of flow over a forested hill (Finnigan and Belcher 2004; Ross and Vosper 2005) this leads to a downwind phase shift in the vertical velocity and pressure fields.

It is not possible to say for certain that the analytical solutions for the pressure field in the long wavelength case with  $\alpha_3 = 1.7$  are accurate since we have no truth to compare with. We know the first order numerical model is not accurate in representing the  $\tau_{zz}$  term and there is no experimental data (field or laboratory) current published with which the analytical results can be compared. However, the good agreement between analytical and numerical models if  $\alpha_3 = 0$  provides confidence in the analysis. Confidence in the closure assumptions with  $\alpha_3 = 1.7$  comes from the fact that it produces good agreement between the analytical solution of BXH and numerical model results from a model with a second order turbulence closure scheme which does accurately predict the  $\tau_{zz}$  term. Although there has been some work testing second order closure model for homogeneous canopy flows (e.g. Ayotte *et al.* 1999; Pinard and Wilson 2001) this has not yet been applied to inhomogeneous canopies, and so it is not possible to do the same comparison as BXH between analytical solution and second order numerical model for the present problem.

### 5. Comparison with flow over a surface of variable roughness

As illustrated in figures 2 and 3 the response of the boundary layer to flow over a surface of variable roughness is very different to that over a canopy of variable density. The results over a rough surface (bottom panels) are obtained using the analytical solution of BXH for the equivalent roughness length

$$z_1 = \frac{z_0}{(1 + \eta e^{ikx})} \quad (61)$$

and so the roughness parameter,  $M$ , in the BXH analytical solution is equal to  $\eta$ . The form of the solution in the middle layer and the outer layer is the same in each case, with only the values of the constants  $B_0$ ,  $C_0$  and  $D_0$  differing. For the longer wavelength change in canopy density (figure 2) the solutions broadly agree for large  $z$ , although there is

a slight phase shift in the  $u$  and  $w$  fields. The agreement is also reflected in the similar phase of the pressure fields between the two analytical solutions (figure 4). In the shear stress layer however the solutions show markedly different behaviour. This difference is due to the fundamentally different behaviour near the surface in the two cases. In the canopy, the horizontal velocity perturbation is  $180^\circ$  out of phase with the canopy density variations since a denser canopy tends to slow down the flow. Continuity shows that the induced vertical velocity field has a phase  $90^\circ$  ahead of the canopy density. Just above the canopy the velocity perturbations are dominated by the canopy-induced flow since  $u$  and  $w$  are continuous at canopy top. There is a large phase shift in  $u$  and  $w$  across the shear stress layer to match the middle and outer layer solutions. In contrast, over a rough surface there is no vertical velocity near the surface and so the velocity perturbations are induced within the inner surface and shear stress layers. An increase in canopy density corresponds to a decrease in the roughness length since the roughness length is proportional to the canopy mixing length (see Eq. 4). Decreasing the roughness will tend to increase the flow speed and so over a rough surface the horizontal velocity perturbations will tend to be in phase with the canopy density changes, the exact opposite of the case where a canopy is included. Similarly the near-surface vertical velocity over a rough surface is  $180^\circ$  out of phase with that over a canopy. The phase of the perturbations are relatively constant with height in the shear stress layer over a rough surface.

As Hobson *et al.* (1999) and others have pointed out, varying only the roughness of a surface is not necessarily realistic. In practice changes in roughness will also be accompanied by changes in the roughness displacement height, which will also impact on the near surface flow. To investigate the impact of displacement height, results from three different numerical simulations are presented for the wide domain in figure 5. The first of these simulations has the canopy modelled explicitly (top plot) as in section 4, the second has a surface with varying

roughness (middle plot) and the third has a surface with both roughness and displacement height varied (bottom plot). The variations in canopy density, roughness and displacement height are chosen to be equivalent so that  $z_0 = (l/\kappa) \exp(-\kappa/\beta)$  and  $d = l/\kappa$  where  $l = 2\beta^3/(Ca)$ . Note that in the numerical model, due to the way the lower boundary condition is coded, the variable displacement height is actually modelled with a variable surface height. As seen in the analytical solutions in figure 2, the model demonstrates significant differences in behaviour between the solution with an explicit canopy and the solution with only a variable roughness length. Inclusion of the effects of variable displacement height significantly alters the near surface (i.e. canopy top) behaviour of the numerical model and gives a vertical velocity field closer to that predicted with an explicit canopy. There are however still significant differences, particularly further above the surface. These differences in the vertical velocity field above the canopy mean that the induced surface pressure field (figure 6) differs between the three runs.

Finally, it is interesting to compare the behaviour of the two analytical solutions in the limit as the canopy approaches a rough surface, i.e. the canopy density is large so that flow into / out of the canopy is negligible. In this limit  $kL_c \rightarrow 0$ . To evaluate the constants in this limit recall that  $kL_c \rightarrow 0 \Rightarrow \zeta_0 \rightarrow 0$ . Taking expansions of the Bessel and Lommel functions for small arguments gives

$$\begin{aligned} K_{00} &\sim -\frac{1}{2} \log(\zeta_0), & \zeta_0 K'_{00} &\sim -\frac{1}{2}, \\ S_{00} &\sim -\frac{1}{16i\zeta_0}, & \zeta_0 S'_{00} &\sim \frac{1}{16i\zeta_0} \end{aligned} \quad (62)$$

and on substituting these we obtain

$$\begin{aligned} A_0 &\rightarrow 2\delta, & B_0 &\rightarrow -\frac{2\kappa^2\delta^2}{U(h_i)}, \\ C_0 &\rightarrow -2ikh_m\delta^2 \frac{i\kappa^2}{U(h_i)}, & D_0 &\rightarrow -\frac{2\kappa^2\delta^2}{U(h_i)} \end{aligned} \quad (63)$$

where  $w_c \rightarrow 0$  in the rough surface limit. In this limit these canopy solution constants all tend to the same values as

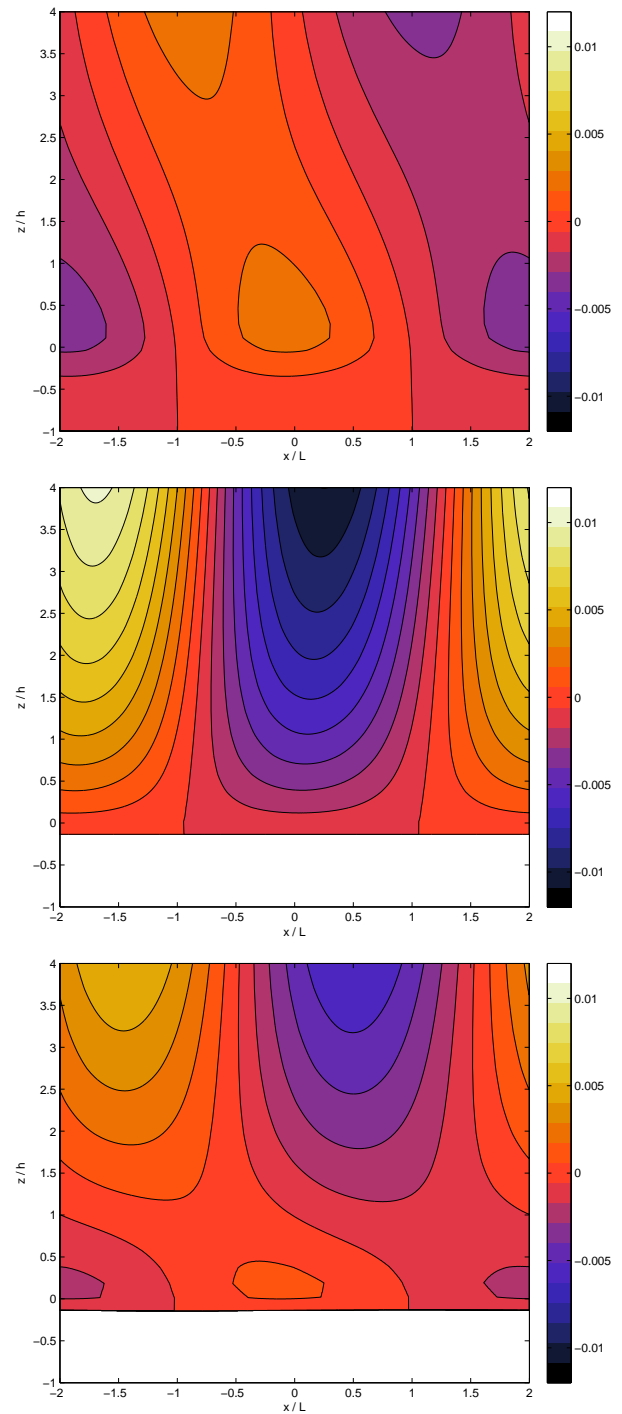


**Figure 5.** Contour plots of the normalised vertical velocity,  $w/(U_0\epsilon\eta/\kappa)$ , from the numerical model for simulations with an explicit canopy of variable density (top), a surface with variable roughness (middle) and a surface with variable roughness and displacement height (bottom). Results are shown for the case with  $L = 1600$  m.

the corresponding constant in the rough surface solution. In the middle and outer layers the form of the solutions in the same in both solutions and so if the constants agree then the solutions are the same in the rough surface limit. In the shear stress layer the solution for  $u$  over a canopy, Eq. (36), contains an additional term involving the Lommel

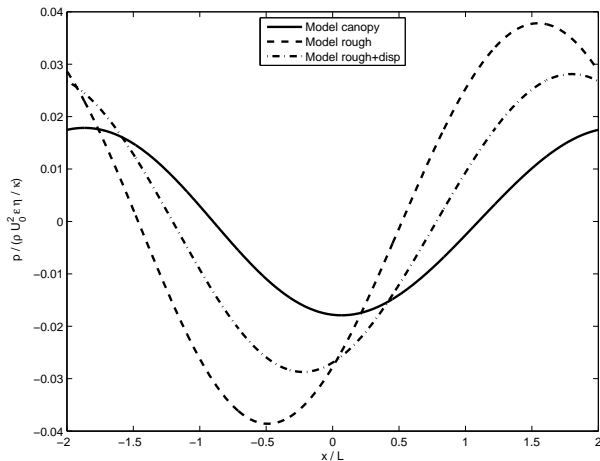


**Figure 6.** Normalised pressure field,  $p/(\rho U_0^2 \epsilon \eta / \kappa)$ , within the canopy as a function of horizontal position. Model results are shown with an explicit canopy, with only variable roughness length and with variable roughness and displacement height. Results are for the slowly varying canopy density with  $L = 1600$  m

function,  $S_{-3,0}$ . For the two solutions to be equivalent this term must be asymptotically small compared to the  $A_0 K_0$  term in the rough surface limit. In the upper parts of the shear stress layer where  $\zeta = O(1)$  then evaluating  $K_0(2e^{i\pi/4})$  and  $iS_{-3,0}(2e^{3i\pi/4})$  shows that these terms are similar in magnitude and phase, and therefore the relative importance of the term involving  $S_{-3,0}$  depends on the ratio  $16\zeta_0/A_0 \sim -8\zeta_0 \log(\zeta_0) \rightarrow 0$  as  $kL_c \rightarrow 0$ . In the upper part of the shear stress layer the two solutions therefore agree asymptotically in the rough surface limit. Lower down in the shear stress layer, near the top of the inner surface layer in the roughness solution of BXH (defined by  $l_s = \sqrt{h_i z_0}$ ) then  $\zeta_s = l_s/h_i = \sqrt{z_0/h_i}$  is small. In this limit the asymptotic expansions presented above for small  $\zeta$  can be used. The ratio of the two terms in the expression for  $u$  is

$$\frac{A_0 K_0}{16i\zeta_0 S_{-3,0}} \sim \frac{\delta \log \zeta}{\zeta_0/\zeta} \sim -\frac{\zeta \log \zeta}{\zeta_0 \log \zeta_0}. \quad (64)$$

The first term ( $A_0 K_0$ ) is larger in magnitude but with the ratio of the two terms approaching -1 as  $\zeta \rightarrow \zeta_0$ . At the top of the inner surface layer then (from BXH) we have  $l_s = (z_0 h_i)^{1/2}$  and so  $\zeta$  is given by

$$\zeta_s = \left(\frac{z_0}{h_i}\right)^{1/2} = \zeta_0^{1/2} e^{-\kappa/(2\beta)} \quad (65)$$

which is still small. Evaluating the ratio of the two terms in  $u$  at this height gives  $\sim (1/2)\zeta_0^{-1/2} e^{-\kappa/(2\beta)} \rightarrow \infty$  as  $\zeta_0 \rightarrow 0$ . So, in the rough surface limit, while the canopy SSL solution and the roughness length SSL do not agree as  $\zeta \rightarrow 0$ , they do converge to the same value in the region  $z > l_s$  where both solutions are valid. In the rough surface limit the leading order shear stress term in the inner surface layer solution of BXH is  $\tau^{(0)} = -1$ . Writing the leading order expression for  $u$  in terms of the SSL variable  $\zeta$  gives

$$u = 1 - \delta (\log \zeta + \delta^{-1} + M) \approx -\delta \log \zeta \quad (66)$$

which matches with the small  $\zeta$  expansion of  $u$  in the canopy solution. So, although the form of the solutions at first appears different, in the rough surface limit  $kL_c \rightarrow 0$  both the rough surface analytical model and the canopy analytical model tend to the same solution.

## 6. Discussion and conclusions

Understanding the effects of heterogeneous vegetation canopies on boundary-layer flow is important in terms of predicting near-surface winds and transport, and is also an important part of parameterizing surface heterogeneities in large-scale climate and weather forecasting models. This paper adds several important insights on this topic.

An analytical model has been developed which predicts the flow induced within and above a canopy with small and slowly changing variations in canopy density. Comparison of the analytical model results with an existing solution for flow over a surface of variable roughness length highlights the importance of the canopy dynamics to this problem. The two models predict entirely different near-surface flows, and even show significant phase differences in the vertical velocity field aloft (see e.g. figure 2). In part this is due to the failure to account for changes in displacement height, but even numerical simulations which include this effect show differences compared to the full canopy model. This is potentially a significant limitation on many existing studies

of the impacts of heterogeneous surface cover (for example Belcher *et al.* 1990; Hobson *et al.* 1999).

The two analytical solutions do agree in the dense canopy limit  $kL_c \rightarrow 0$  (see section 5), although convergence is slow and so practically  $kL_c$  must be very small for the solutions to agree, i.e. it requires very dense canopies ( $L_c \ll 1$ ) or very slowly varying canopy densities ( $k \ll 1$ ). This has implications for when a forest can be well represented with just a roughness length and when a full canopy model may be required. Many real world heterogeneous forest canopies lie outside the dense canopy regime and therefore the analytical canopy solution may be useful. There is still a lack of experimental data, either from lab studies or from the field, with which to compare this theory. Results from such experimental studies would be very welcome in helping to confirm the theoretical results presented here.

A further point highlighted by this study, as well as the previous study by Belcher *et al.* (1990) is the importance of the parameterization of the  $\tau_{zz}$  terms in the inner layer. Over forest canopies there is still some uncertainty in how this should be parameterized, with the observations suggesting that the constant ratio  $\tau_{zz}/\tau$  often used in the boundary layer is not applicable in the RSL above a forest canopy. The analytical model does provide a framework in which to study the effects of different parameterizations. It also highlights that mixing length closure models are unlikely to fully capture the details of such flows. This again is likely to be a limitation of previous studies. The lack of reliable second order numerical models for inhomogeneous canopy flows is hampering our ability to investigate problems such as this further.

Finally, the breakdown of the analytical model for small wavelength variations demonstrates the increased importance of canopy flows at these small scales, just as for flow over a forested hill (see Finnigan and Belcher 2004; Ross and Vosper 2005). In this case it is the more rapid spatial changes in the canopy density which lead to more rapid acceleration and deceleration of the flow and hence induce stronger vertical velocities in the canopy.

The larger induced velocities then violate the assumption in the analytical model that the advection terms are not important at leading order. In some practical applications canopy densities do vary over relatively short distances, and so the analytical solution as it stands may not be directly applicable. The scaling arguments and physical insight gained from this work will however help to explain the dominant physical processes in such cases.

One important difference between the analytical solution developed here and the solution for flow over a forested hill given by Finnigan and Belcher (2004) is that for moderate depth canopies the solution remains linear throughout the canopy, whereas over a hill the deep canopy solution is inherently non-linear. This has the important advantage that the linear solutions developed here for a single wavelength for the canopy variations can be added together to give solutions for arbitrary horizontal variations in canopy density, provided that the linear analytical solution is valid for all the different modes considered. Finally, the similarity of this solution to the solution of Finnigan and Belcher (2004) over a hill offers possibilities for developing a unified analytical model include the effects of both heterogeneous terrain and canopy density. This might be particularly interesting for studying pressure drag over hills since the pressure field induced by variations in canopy density might well be out of phase with the topography, and therefore even a relatively small induced pressure field could have a noticeable impact on the drag.

#### **Appendix A. Vertical velocity and streamfunction within the canopy**

For the non-linear solution in a deep canopy the vertical velocity can be obtained in exactly the same manner as in FB. The linear part of the vertical velocity from the upper canopy,  $w_u$ , is given in section 2.1.2. The non-linear part,  $w_d$ , is derived separately in 4 different regions depending on the sign of the pressure gradient and the height at which the flow becomes reversed (see table II). The flow reverses

Table II. Regions of the canopy

Region	Definition
1	$dp_0/dx < 0$
2	$dp_0/dx > 0, h <  Z_s(x) $
3	$dp_0/dx > 0, h >  Z_s(x) , z < Z_s(x)$
4	$dp_0/dx > 0, h >  Z_s(x) , z > Z_s(x)$

when  $U_B^2 = L_c dp_0/dx$  at a height

$$Z_s = \frac{l}{2\beta} \ln \left( \frac{L_c dp_0/dx}{U_h^2} \right). \quad (67)$$

Correcting the mistake in  $I_6$  from FB noted in Ross and Vosper (2005), the vertical velocity in the canopy is given by

$$w_{d1} = \frac{d^2 p_0}{dx^2} \frac{L_c l}{2\beta} (I_4(z) - I_4(-h)) \quad (68)$$

$$w_{d2} = \frac{d^2 p_0}{dx^2} \frac{L_c l}{2\beta} (I_5(z) - I_5(-h)) \quad (69)$$

$$w_{d3} = \frac{d^2 p_0}{dx^2} \frac{L_c l}{2\beta} (I_6(z) - I_6(-h)) \quad (70)$$

$$w_{d4} = \frac{d^2 p_0}{dx^2} \frac{L_c l}{2\beta} (I_5(z) - I_6(-h)) \quad (71)$$

where

$$I_4(z) = \frac{1}{2b} \ln \left\{ \frac{(U_B^2 + b^2)^{1/2} - b}{(U_B^2 + b^2)^{1/2} + b} \right\} \quad (72)$$

$$I_5(z) = \frac{1}{c} \arccos \left( \frac{c}{U_B} \right) \quad (73)$$

$$I_6(z) = \frac{1}{c} \ln \left\{ \frac{(c + U_b)^{1/2} - (c - U_B)^{1/2}}{(c + U_b)^{1/2} + (c - U_B)^{1/2}} \right\} \quad (74)$$

$$b^2 = -L_c \frac{dp_0}{dx}, \quad c^2 = L_c \frac{dp_0}{dx}. \quad (75)$$

In this case, unlike in FB, the leading order pressure field is not known a priori and so the phase is not known until the full solution for flow above the canopy is found.

Similarly, just as in FB, the streamfunction in the canopy can be obtained by integrating either the  $u$  or  $w$  fields. The streamfunction is split into 3 components - the mean flow component,  $\psi_0$ , the part associated with the upper canopy solution,  $\psi_u$  and the part associated with the non-linear deep-canopy solution. The mean flow and upper canopy

parts are

$$\psi_0 = \frac{l_0}{\beta} (U_B(z) - U_B(-h)), \quad (76)$$

$$\psi_u = U_0 \frac{\epsilon \eta}{\kappa} 2\beta^2 L_c \exp(ikx) \left( \frac{\kappa}{\beta} (Z - 1) e^Z + \frac{\kappa}{\beta} \left( 1 + \frac{\beta h}{l_0} \right) e^{-\beta h/l_0} + A \left( e^Z - e^{-\beta h/l_0} \right) \right). \quad (77)$$

The deep canopy streamfunction is the same as in FB (correcting a sign error in the second term of  $I_3$ ) and is given separately in the different regions (1-4) of the canopy by

$$\psi_{d1} = \frac{l_0}{\beta} (I_1(z) - I_1(-h)) \quad (78)$$

$$\psi_{d2} = \frac{l_0}{\beta} (I_2(z) - I_2(-h)) \quad (79)$$

$$\psi_{d3} = \frac{l_0}{\beta} (I_3(z) - I_3(-h)) \quad (80)$$

$$\psi_{d4} = \frac{l_0}{\beta} (I_2(z) - I_3(-h)) \quad (81)$$

where

$$I_1(z) = (U_B^2 + b^2)^{1/2} + \frac{1}{2} b \ln \left\{ \frac{(U_B^2 + b^2)^{1/2} - b}{(U_B^2 + b^2)^{1/2} + b} \right\} \quad (82)$$

$$I_2(z) = (U_B^2 - c^2)^{1/2} - c \arccos \left( \frac{c}{U_B} \right) \quad (83)$$

$$I_3(z) = - (c^2 - U_B^2)^{1/2} - c \ln \left\{ \frac{(c + U_b)^{1/2} - (c - U_b)^{1/2}}{(c + U_b)^{1/2} + (c - U_b)^{1/2}} \right\}. \quad (84)$$

## References

- Ayotte KW, Finnigan JJ, Raupach MR. 1999. A second-order closure for neutrally stratified vegetative canopy flows. *Boundary-Layer Meteorol.* **90**: 189–216, doi:10.1023/A:1001722609229.
- Belcher SE, Jerram N, Hunt JCR. 2003. Adjustment of a turbulent boundary layer to a canopy of roughness elements. *J. Fluid Mech.* **488**: 369–398, doi:10.1017/S0022112003005019.
- Belcher SE, Newley TMJ, Hunt JCR. 1993. The drag on an undulating surface induced by the flow of a turbulent boundary layer. *J. Fluid Mech.* **249**: 557–596, doi:10.1017/S0022112093001296.

- Belcher SE, Xu DP, Hunt JCR. 1990. The response of a turbulent boundary layer to arbitrarily distributed two-dimensional roughness changes. *Quart. J. Roy. Meteorol. Soc.* **116**: 611–635, doi:10.1002/qj.49711649306.
- Coccal O, Belcher SE. 2004. A canopy model of mean winds through urban areas. *Quart. J. Roy. Meteorol. Soc.* **130**: 1349–1372, doi:10.1256/qj.03.40.
- Dupont S, Brunet Y. 2008. Edge flow and canopy structure: A large-eddy simulation study. *Boundary-Layer Meteorol.* **126**: 51–71, doi:10.1007/s10546-007-9216-3.
- Dupont S, Brunet Y. 2009. Coherent structures in canopy edge flow: a large-eddy simulation study. *J. Fluid Mech.* **630**: 93–128, doi:10.1017/S0022112009006739.
- Dupont S, Brunet Y, Finnigan JJ. 2008. Large-eddy simulation of turbulent flow over a forested hill: Validation and coherent structure identification. *Quart. J. Roy. Meteorol. Soc.* **134**: 1911–1929, doi:10.1002/qj.328.
- Finnigan JJ. 2000. Turbulence in plant canopies. *Annu. Rev. Fluid Mech.* **32**: 519–571, doi:10.1146/annurev.fluid.32.1.519.
- Finnigan JJ, Belcher SE. 2004. Flow over a hill covered with a plant canopy. *Quart. J. Roy. Meteorol. Soc.* **130**: 1–29, doi:10.1256/qj.02.177.
- Hobson JM, Wood N, Brown AR. 1999. Large-eddy simulations of neutrally stratified flow over surfaces with spatially varying roughness length. *Quart. J. Roy. Meteorol. Soc.* **125**: 1937–1958, doi:10.1256/smsqj.55802.
- Hunt JCR, Leibovich S, Richards KJ. 1988. Turbulent shear flow over low hills. *Quart. J. Roy. Meteorol. Soc.* **114**: 1435–1470, doi:10.1002/qj.49711448405.
- Irvine MR, Gardiner BA, Hill MK. 1997. The evolution of turbulence across a forest edge. *Boundary-Layer Meteorol.* **84**: 467–496, doi:10.1023/A:1000453031036.
- Lee X. 2000. Air motion within and above forest vegetation in non-ideal conditions. *Forest Ecology and Management* **135**: 3–18, doi:10.1016/S0378-1127(00)00294-2.
- Morse AP, Gardiner BA, Marshall BJ. 2002. Mechanisms controlling turbulence development across a forest edge. *Boundary-Layer Meteorol.* **103**: 227–251, doi:10.1023/A:1014507727784.
- Olver FWJ, Lozier DW, Boisvert RF, Clark CW (eds). 2010. *NIST handbook of mathematical functions*. Cambridge University Press, 1st edn.
- Pinard JDJP, Wilson JD. 2001. First- and second-order closure models for wind in a plant canopy. *J. Appl. Meteor.* **40**(10): 1762–1768, doi:10.1175/1520-0450(2001)040<1762:FASOCM>2.0.CO;2.
- Romniger JT, Nepf HM. 2011. Flow adjustment and interior flow associated with a rectangular porous obstruction. *J. Fluid Mech.* **680**: 636–659, doi:10.1017/jfm.2011.199.
- Ross AN. 2008. Large eddy simulations of flow over forested ridges. *Boundary-Layer Meteorol.* **128**: 59–76, doi:10.1007/s10546-008-9278-x.
- Ross AN. 2011. Scalar transport over forested hills. *Boundary-Layer Meteorol.* **141**: 179–199, doi:10.1007/s10546-011-9628-y.
- Ross AN, Vosper SB. 2005. Neutral turbulent flow over forested hills. *Quart. J. Roy. Meteorol. Soc.* **131**: 1841–1862, doi:10.1256/qj.04.129.
- Yang B, Raupach MR, Shaw RH, Tha K, Paw U KT, Morse AP. 2006. Large-eddy simulation of turbulent flow across a forest edge. Part 1: Flow statistics. *Boundary-Layer Meteorol.* **120**(3): 377–412, doi:10.1007/s10546-006-9057-5.